Published in final edited form as:
Clin Exp Metastasis. 2014 January ; 31(1): 67–79. doi:10.1007/s10585-013-9610-9.

Pre-treatment of mice with tumor-conditioned media accelerates metastasis to lymph nodes and lungs: a new spontaneous breast cancer metastasis model

Esak Lee[1,2], **Niranjan B. Pandey**[1], and **Aleksander S. Popel**[1,2,3]

[1]Department of Biomedical Engineering, Johns Hopkins University School of Medicine, Baltimore, MD 21205, USA.

[2]Department of Chemical and Biomolecular Engineering, School of Engineering, Johns Hopkins University, Baltimore, MD 21218, USA.

[3]Department of Oncology and the Sidney Kimmel Comprehensive Cancer Center, Johns Hopkins University School of Medicine, Baltimore, MD 21231, USA.

Abstract

Current spontaneous metastasis models require a long period of observation after establishment of primary tumors to see significant metastatic progression. The degree of metastasis is not consistent among animals: this is problematic since it requires the use of a large number of animals to obtain reliable statistics. Here we report that pre-treatment of animals with tumor-conditioned media (TCM) consistently accelerates spontaneous metastasis in breast cancer. An inguinal breast tumor model facilitated by TCM showed robust anterior metastasis to the axillary and brachial lymph nodes (LN), and the lungs compared to the serum-free media (SFM) treated group. The LN in TCM-treated animals showed enhanced angiogenesis and lymphangiogenesis. Primary tumors and lungs in TCM-treated animals showed enhanced lymphangiogenesis with no significant change in angiogenesis. TCM-treated animals also showed metastatic dissemination to abdomen from the primary injection site: this would generally enhance metastasis to other organs. In sum, the addition of TCM pre-treatment to current metastasis models results in accelerated and robust metastasis which would enable more efficient evaluation of anti-metastatic agents.

Keywords

Breast cancer; spontaneous metastasis; accelerated metastasis model; triple negative breast cancer; MDA-MB-231; SUM-149

Introduction

The development of anti-metastatic agents has been hampered by the lack of spontaneous metastasis models for preclinical evaluation of therapeutic agents. Establishing spontaneous metastasis models has been difficult because of the dependence of spontaneous metastasis on diverse factors such as the degree of tumor growth [1], tumor angiogenesis [2], lymphatic networks [3], aggressiveness or invasiveness of cancer cells [4], and the condition of pre-metastatic niches [5]. The effects of these factors are quite unpredictable in tumor-bearing animals thus causing inconsistent metastatic progression and inefficient metastasis.

Correspondence to: Dr. Aleksander S. Popel, Department of Biomedical Engineering, Johns Hopkins University School of Medicine, 611 Traylor building, 720 Rutland Avenue, Baltimore, MD 21205, United States, Tel: 1-410-955-6419, Fax: 1-410-614-8796, apopel@jhu.edu.

Though experimental mouse models for metastasis such as the tail-vein injection model and the intracardiac injection model develop consistent metastases in a short time, these models have drawbacks: they reflect only blood vessel-mediated metastasis, and are triggered by artificially injected cancer cells into the blood stream. Analysis of preclinical and clinical studies shows that metastasis occurs through both the lymphatic vessels and the blood vessels [6, 7]. Thus, there is an unmet need for the development of spontaneous metastasis models in which lymphogenous and hematogenous metastasis occur rapidly and consistently.

We previously developed a tumor-conditioned regional lymph node (LN) model by injecting tumor-conditioned media (TCM) subcutaneously into animals [8]. This model simulates the conditioning of tumor-draining LN or tumor-influenced organs by primary tumor-secreted factors which are transported through the lymphatic and blood vessels [9–12]. In that study we showed that LN in the TCM pre-treated animals had enhanced angiogenesis and lymphangiogenesis compared to those in serum-free media (SFM) treated animals [8]. We hypothesize that this “TCM pre-treatment” would influence tumors and distal organs, thus facilitating tumor metastasis. In this study we add the “TCM pre-treatment” step to an established metastasis model to develop a more efficient spontaneous breast cancer metastasis model. Although we discuss possible mechanisms of action by which metastasis is accelerated, the primary goal of this study is to establish the methodology; a study of the molecular mechanisms in further detail will be presented elsewhere. The new model adds to the collection of mouse models for breast cancer metastasis [13, 14].

Materials and Methods

Cell culture

Human triple-negative breast cancer (TNBC) cells MDA-MB-231 and SUM-149 were supplied by Dr. Zaver Bhujwalla (Radiology and Oncology, Johns Hopkins Medical Institutions). MDA-MB-231-luc-D3H2LN was purchased from Caliper (Hopkinton, MA) [15]. MDA-MB-231 and MDA-MB-231-luc-D3H2LN cells were propagated in RPMI-1640 media (Gibco, Carlsbad, CA) supplemented with 10% Fetal Bovine Serum (FBS, Sigma Aldrich, St. Louis, MO) and 1% penicillin streptomycin (Gibco). SUM-149 cells were cultured in F-12 media (Corning, Manassas, VA) supplemented with 5% FBS (Sigma Aldrich), 1 ng/ml hydrocortisone (Sigma Aldrich), 5 μg/ml insulin (Sigma Aldrich), 0.1mM 4-(2-Hydroxyethyl)-1-piperazineethanesulfonic acid (HEPES) (Gibco). Lymphatic endothelial cells (LEC) and microvascular endothelial cells (MEC) were purchased from Lonza (Walkersville, MD). LEC and MEC were propagated in microvascular endothelial cell growth medium-2 (EGM-2MV, Lonza).

Preparation of tumor-conditioned media (TCM)

MDA-MB-231 cells or SUM-149 cells in complete media (RPMI-1640 or F-12 media with supplements) were plated on T175 tissue culture plates. When the cells formed a confluent monolayer, the complete media was removed and the cells were carefully rinsed with serum-free media (SFM, RPMI-1640 or F-12 without supplements). 8 ml of the same SFM was added to the cells. After 24 h incubation, the supernatant was collected, centrifuged, and filtered through 0.2 μm syringe filters (Corning, Tewksbury, MA). The resulting tumor-conditioned media (TCM) was stored in aliquots at −80°C to avoid multiple freeze thaws.

Cell migration assays

Tumor cell migration was assessed by using the Oris™ cell migration kit (Platypus, Madison, WI). MDA-MB-231 cells were pre-labeled with Cell Tracker Green (Invitrogen, Carlsbad, CA) according to the manufacturer’s protocol. 50,000 labeled cancer cells in

complete media were added to each well of a 96-well plate containing stoppers to prevent the cells from settling in the center region of the wells. Cells were allowed to adhere for 4 h, after which the stoppers were removed. TCM or SFM (100 μl) was added, and the cells that migrated to the center of the well were quantified by measuring the fluorescence at 485/530 nm on a Victor V plate reader (PerkinElmer, Salem, MA). The migrated cells were also visualized by imaging on the Eclipse T-100 fluorescence microscope (Nikon, Brighton, MI).

Tube formation assay

50 μl Matrigel (Growth factor reduced, BD Biosciences, Bedford, MA), thawed on the ice at 4°C overnight, was loaded in each well of a pre-cooled 96-well plate, and the plate was incubated at 37°C for 30 min. 15,000 lymphatic endothelial cells (LEC) and microvascular endothelial cells (MEC) in 100 μl MDA-MB-231 TCM or SUM-149 TCM were added on top of the matrix in the 96-well plate. For controls, LEC and MEC in endothelial cell growth media (EGM-2MV, Lonza) or serum-free media (EBM-2, endothelial basal media-2, Lonza) were also loaded. The plate was then incubated at 37°C, and the wells were imaged using a Nikon microscope at 14 h (Nikon Instruments Inc., Melville, NY).

Lymph node assay

Athymic nude mice were administered 50 μl MDA-MB-231 tumor conditioned media (TCM) or serum-free media (SFM) subcutaneously on a daily basis. After 14 days of administration, mice were euthanized and the axillary and brachial lymph nodes (LN) were excised from each animal. We rinsed the LN in cold PBS and the rinsed LN were placed in 100 μl tissue lysis buffer containing 150 mM NaCl, 50 mM Tris HCl, 1 mM EDTA, 1% Triton-X, phosphatase inhibitors cocktail-2/3 and protease inhibitors (Sigma), homogenized using a tissue grinder (Pyrex Potter-Elvehjem Tissue Grinders with PTFE Pestle), and incubated at 4°C for 2 h. The lysed samples were spun to remove cell membranes and debris for 40 min at 14,000 rpm. LN lysate was separated with SDS-PAGE and transferred to nitrocellulose blots (Invitrogen, Carlsbad, CA). We blocked for 1 h with 5% non-fat milk in TBST (1× TBS with 0.1% Tween) and probed with antibodies of interest including MECA-79 (Santa Cruz Biotechnologies, Inc.), p-VEGFR-2 (Y1175), p-EGFR (Y1068), GAPDH (Cell Signaling Technologies, Inc.). GAPDH was used as a loading control and the secondary antibodies (GE Healthcare) were added at 1:2000 dilution and protein bands detected with chemiluminescence detection reagent (GE Healthcare).

The accelerated spontaneous metastasis model

Animal protocols described in this study were approved by the Institutional Care and Use Committee at the Johns Hopkins Medical Institutions. Before tumor inoculation, we pre-treated athymic nude mice (female, 5–6 weeks, 18–20 g) by injecting 50 μl tumor-conditioned media (TCM) or serum-free media (SFM) subcutaneously through the scruff for 2 weeks as described previously [8]. We measured the animals' body weight in the duration of the experiment to determine if there was TCM-induced toxicity in the animals. After 2 weeks of TCM treatment, MDA-MB-231-luc-D3H2LN tumor xenografts were established in the same animals. MDA-MB-231-luc-D3H2LN breast cancer cells (2×10^6) in 50 μl complete media (RPMI-1640 supplemented with 10% FBS), and 50 μl Matrigel (High Concentrated, BD Biosciences) were well mixed and injected into the upper inguinal mammary fat pad of the animals under anesthesia (50 mg/kg ketamine + 5 mg/kg acepromazine in PBS, 50 μl/animal, intraperitoneally dosed). We did not perform a mastectomy of the primary inguinal mammary tumors as the tumor injection site is sufficiently far from the anterior organs, metastasis to which we were interested in observing. The primary tumor size was measured by using a caliper, and the volume was calculated, using the formula: $V = 0.52 \times a \times b^2$, where 'a' is the long axis, and 'b' is the short axis of the tumor. We also imaged animals every week to track anterior tumor

metastases, using the IVIS Xenogen 200 optical imager (Xenogen, Alameda, CA) after intraperitoneal injection of D-luciferin (Caliper, 150 mg/kg). 100 μl D-luciferin (twice diluted) was intraperitoneally dosed in both sides of the abdomen (total 200 μl/animals) to prevent i.p. injection failure [15]. After 4 weeks, the axillary and brachial LN, the lungs, and the brain were harvested and bathed in D-luciferin solution for 3 min and placed in the IVIS imager to detect metastases ex vivo. Luciferase-mediated photon flux was quantified by using Living Image® 3D Analysis (Xenogen), and the average photon flux was obtained from 8 lungs, 8 brains, and 14–16 lymph nodes as described before [16]. In case of animals showing intra-abdominal metastases, ex-vivo images of abdominal organs, including stomach, spleen, kidney, liver, and intestine, were obtained using the IVIS imager.

We also tested another triple-negative breast cancer (TNBC) cell line, SUM-149 by using the same metastasis model as above, to demonstrate the application of the model to other cell types of breast cancer. Because luciferase-transfected SUM-149 are not available, instead of using the IVIS imager, we performed 3,3' diaminobenzidine (DAB) mediated immunohistochemistry with cytokeratin 7 antibodies (anti-CK7) and human proliferating cell nuclear antigen (PCNA) antibodies on the lungs and the LN. These organs were harvested after 6 weeks of tumor inoculation when the tumor size in both TCM and SFM-treated groups reaches approximately 1,000 mm^3, which is the same tumor size in the MDA-MB-231 model above (4 weeks). We harvested 10 lungs and 40 LN (2 axillary and 2 brachial LN, each mouse) from each group of animals (N=10). The organs were fixed, frozen and sectioned into 10 μm thick slices, yielding 3 slides from the top, the middle, and the bottom of the organs, resulting in a total of 30 slides for lungs and 120 slides for LN in each group.

Immunofluorescence and immunohistochemistry

For immunofluorescence, tumors, LN, and lungs fixed in 4% formalin were placed in 30% sucrose solution in PBS, incubated overnight at 4°C, and frozen in the Tissue-Tek Optimal Cutting Temperature (O.C.T.) compound (Sakura, Tokyo, Japan). Sections of 10-μm thickness were cut at −20°C. After blocking with 5% normal goat serum (Jackson ImmunoResearch, West Grove, PA) in PBST (1× PBS with 0.3% Triton) for 1 h at room temperature, the sections were treated with one or more of the following primary antibodies overnight at 4°C: rabbit anti-mouse LYVE-1 antibody (lymphatic vessel endothelial hyaluronan receptor-1, 1:200, AngioBio, Del Mar, CA), rat anti-mouse CD31 (1:100, BD Pharmingen, San Jose, CA), and rat anti-lectin FITC (fluorescein isothiocyanate) (1:100, Sigma Aldrich). After 3 rinses with PBST, sections were incubated for 1 h at room temperature with one or more of the secondary antibodies: fluorescein isothiocyanate (FITC)-conjugated goat anti-rat antibody, rhodamine-conjugated goat anti-rat antibody, Cy3-conjugated goat anti-rabbit antibody (all three from Jackson ImmunoResearch), Alexa Fluor 647 goat anti-rabbit antibody, and Alexa Fluor 488 goat anti-rabbit antibody (all two from Cell Signaling Technology, Danvers, MA). The samples were washed with PBST 3 times and DAPI (4',6-diamidino-2-phenylindole, 1:10,000, Roche, Indianapolis, IN) was used for nuclear staining for 5 min at room temperature. The samples were washed with PBST 1 time, and mounted with the ProLong Gold anti-fade reagent (Invitrogen, Carlsbad, CA). Fluorescent signals were visualized and digital images were obtained, using a LSM-510 confocal microscope equipped with argon and helium-neon lasers (Carl Zeiss, Baltimore, MD). We quantified the images, averaging the pixel intensity of 12 images that are randomly selected (10× magnification) in each group by using ImageJ (National Institutes of Health, Bethesda, MD). For immunohistochemistry, LN and lungs from SUM-149 xenograft mice were fixed, frozen and sectioned as above. After blocking with 5% goat serum in PBST for 1 h at room temperature, the sections were treated with mouse anti-cytokeratin 7 antibodies (1:200, Sigma Aldrich) or mouse anti-human PCNA antibodies

(1:2000, BD Pharmingen) overnight at 4°C. After 4 rinses with PBST, the sections were incubated for 30 min at room temperature with SignalStain® Boost IHC Detection Reagent (HRP-conjugated, for mouse antibody detection, Cell Signaling). The samples were washed with PBST 3 times, and treated with SignalStain® DAB Substrate (Cell Signaling) for 1 min. 0.1% Hematoxylin Solution (Sigma-Aldrich) was used for counterstaining. After washing with tap water, the slides were incubated in 0.1% Sodium bicarbonate (Sigma) for 1 min and rinsed with tap water. Dehydrated slides were mounted with glycerol, and covered with a glass slide. Slides were examined on the Olympus BX51TF with DP70 color camera (Olympus, Japan). Because the DAB pixel density from three randomly selected sections of each organ cannot represent the exact metastatic rate, we did not average the pixel density but determined how many lungs (from 10 lungs) or LN (from 20 ax-LN and 20 br-LN) were cancer cell positive by anti-CK-7 and anti-human PCNA.

Statistical analysis

Error bars correspond to SEM. Differences between a control and treated groups are regarded as significant when p is less than 0.05 using the Student's t-test.

Results

Accelerated metastasis to the LN and the lungs by pre-treatment of animals with TCM

We separated mice into two groups: "TCM group", animals pre-treated with tumor-conditioned media (TCM); and "SFM group", animals pre-treated with serum-free media (SFM). After two weeks of TCM (or SFM) treatment, 2×10^6 MDA-MB-231-luc-D3H2LN or SUM-149 cells were inoculated into the upper mammary fat pad in the inguinal region of the animals. In the MDA-MB-231-luc-D3H2LN model, we assessed anterior metastases every week using the IVIS imager: every animal in the "TCM group" had metastases anterior in the anterior organs within 4 weeks, whereas the "SFM group" did not show significant distant metastasis (1 out of 8 mice at 4 weeks) (Fig. 1A). However, TCM pre-treatment did not influence the body weights of the animals and the mean tumor volume (Figs. 1B and 1C). Four weeks of tumor inoculation, when the size of primary tumors was approximately 1,000 mm^3 (Fig. 1C), the animals were euthanized, and the axillary and brachial LN, the lungs, and the brains were excised. The luciferase-expressing tumor cells in these organs were detected ex vivo (Figs. 1D and 1E). Luciferase-mediated metastatic signals, the averaged photon flux from metastatic tumor cells in the organs (8 lungs, 8 brains, and 14–16 LN) were measured. LN and lungs showed significantly enhanced metastatic signals, however, brains showed no difference (Fig 1E).

Additionally, SUM-149 xenograft models were treated with TCM prepared from SUM-149 cells or serum-free media (SFM, F-12 media without supplements). In the SUM-149 model, we assessed metastasis by performing immunohistochemistry with anticytokeratin 7 and anti-human PCNA antibodies (Figs. 2 and 3). Tumor growth data showed that primary tumor size was not influenced by TCM pre-treatment (Fig. 2A). SFM-treated animals had 4 metastasized axillary LN (ax-LN) and 7 metastasized brachial LN (br-LN) out of 20 LN, respectively. Notably, TCM pre-treated group showed increased LN metastasis with metastases in 13 ax-LN and 16 br-LN (Fig. 2B). We also observed that TCM-treated LN exhibited lymphadenopathy (swollen LN) with transparent fluid inside of the LN. LN from serum-free media (SFM) treated animals looked normal (Fig. 2C). Immunohistochemistry results showed that TCM-treated LN are highly metastasized and the area of lymphadenopathy is spatially associated with metastasized tumor cells (represented by black arrows) that are detected by anti-CK7 and anti-human PCNA (Figs. 2D and 2E). In animals with SUM-149 tumors, the TCM pre-treated group showed profound lung metastases in the 9 lungs out of 10 lungs, but the SFM-treated control showed metastasis in 3 out of 10 lungs

(Fig. 3A). Macroscopic images show metastatic tumor nodules on the lung surface in the TCM-treated group (Fig. 3B). Immunohistochemistry confirmed anti-cytokeratin 7 and anti-human PCNA positive tumor cells in the TCM-treated lung tissues (Figs. 3C and 3D).

TCM pre-treatment promotes lymphangiogenesis in primary tumors

We performed immunofluorescence on MDA-MB-231 primary tumors from the "TCM group" or "SFM group". The primary tumors were excised 4 weeks after tumor inoculation on the inguinal mammary fat pads. Anti-mouse LYVE-1 (with a green secondary antibody) and anti-mouse CD31 (with a red secondary antibody) antibodies were used to detect the lymphatic vessels and the blood vessels in the tumors. TCM pre-treatment dramatically increased the number of lymphatic vessels in the tumor by 4.68 fold (**$P < 0.01$) compared to the SFM-treated group (Figs. 4A and 4C). However, blood vessel density in the tumors was not influenced by TCM treatment (Figs. 4B and 4C).

TCM-treatment induces lymphangiogenesis in lungs and LN, angiogenesis was enhanced in the LN

We also analyzed the lungs and the LN from TCM or SFM pre-treated animals (Fig. 5). In this set of experiments we did not establish primary inguinal tumors but just pre-treated animals with TCM (MDA-MB-231 cell derived) or SFM for two weeks. This was done because we wanted to investigate the change in blood vascular capillaries or lymphatics by TCM treatment and not by metastasized tumor cells or primary tumors. The lungs of animals treated with TCM had 2.62 times more lymphatic vessels than the lungs of SFM-treated animals (*$P < 0.05$); there were no significant differences in blood vessel density stained with anti-CD31 and anti-lectin (Figs. 5A and 5C). We analyzed LN from TCM or SFM treated animals (Figs. 5B and 5D). The brachial LNs of the TCM-treated animals had 3.20 times as many lymphatic vessels and 1.74 times as many blood vessels compared to the brachial LNs of SFM-treated animals (**$P < 0.01$ in LVs, *$P < 0.05$ in BVs) (Figs. 5B and 5D). Enhanced angiogenesis in the LN was further analyzed by performing western blot assays with LN tissue lysates (Figs. 6A and 6B). MECA-79 was used to measure LN-specific endothelium (HEV: high endothelial venules). Phosphorylation of vascular endothelial growth factor receptor 2 (VEGFR-2) and epidermal growth factor receptor (EGFR) was additionally assessed to examine TCM-mediated proangiogenic signaling. The amount of MECA-79 and presumably the number of endothelial cells was changed by 4.1 fold in axillary LN and by 6.9 fold in brachial LN after TCM treatment. Phosphorylation of VEGFR-2 was also increased 10.5 fold in axillary LN and 5.7 fold in brachial LN. Phosphorylation of EGFR was increased 3.3 fold in axillary LN and 3.0 fold in brachial LN (Figs. 6A and 6B).

TCM exhibits lymphangiogenic and angiogenic potential in tube formation assays

Based on the result of immunofluorescence that TCM promotes lymphangiogenesis or angiogenesis in the LN and the lungs (Fig. 5), we assessed TCM in tube formation by lymphatic endothelial cells (LEC) and microvascular endothelial cells (MEC), evaluating the effect of TCM in functional lymphangiogenesis and angiogenesis (Fig. 6C). For controls, normal endothelial growth media (EGM-2MV) and serum-free media (SFM) were employed. TCM prepared from MDA-MB-231 cells profoundly promoted MEC and LEC tubes compared to SFM in which the cells failed to form tubes. The tubes formed in TCM were comparable to the tubular network induced by normal growth media (EGM-2MV). SUM-149 had moderate angiogenic and lymphangiogenic activity, which was weaker than the induction by MDA-MB-231 TCM (Fig. 6C).

TCM enhances tumor cell motility and metastasis to the abdomen

We assessed MDA-MB-231 cell migration induced by TCM or by SFM. TCM treatment enhanced tumor cell motility 3.13 fold at 9 h (*$P < 0.05$), and 5.26 fold at 18 h (**$P < 0.01$) compared to SFM treatment (Figs. 7A and 7B). We also observed TCM or SFM pre-treated animals, comparing of intra-abdominal metastasis from the primary site, after 4 weeks of the primary tumor inoculation. Cancer cells from the primary tumors were disseminated to the abdominal site in five animals (out of 8 mice total) when the mice were pre-treated with TCM (Fig. 7C). Two mice (out of 8) showed intra-abdominal metastases when they were pre-treated with SFM. Internal organs placed in the abdominal area, including stomach, spleen, kidney, liver, and intestine were excised and examined under the IVIS Xenogen imager. Metastases were detected in the stomach, spleen, liver, jejunum and duodenum (Fig. 7C).

Discussion

In the present study we showed that TCM-treated animals had accelerated spontaneous metastasis to the LN and the lungs in two different triple-negative breast cancer (TNBC) models: MDA-MB-231 and SUM-149 mammary fat pad xenografts (Figs. 1–3). These metastases spontaneously disseminated from the primary inguinal tumors within 4 weeks in the MDA-MB-231 model and 6 weeks in the SUM-149 model, which is significantly faster than serum-free media (SFM) treated animals as well as current spontaneous metastasis models that take more than 7 – 10 weeks [15]. We observed that TCM pre-treatment followed by tumor inoculation facilitated spontaneous metastasis by influencing lymphangiogenesis and angiogenesis in the primary tumors and pre-metastatic organs. Primary tumors in the animals that had been pre-treated with TCM showed more lymphatic vessels in their peripheral areas (Fig. 4). The increased metastasis seen in animals that underwent TCM pre-treatment could be partly explained by the higher number of peritumoral lymphatic vessels which could facilitate the outflow of tumor cells from the tumor. We also observed that these peritumoral lymphatic vessels had lumens, which would be critical for the dissemination of tumor cells through these vessels (Fig. 4A). It has been reported that the lymphatics in the interior of the tumor do not function in lymphatic metastasis [17]. This is thought to be the case because the lumens of the intratumoral lymphatic vessels tend to be compressed by the interstitial pressure of the tumor, making metastatic dissemination through these vessels impossible. Interestingly, tumor angiogenesis was not influenced by TCM treatment (Figs. 4B and 4C). This is consistent with the result that primary tumor size is not changed by TCM treatment (Figs. 1C and 2A).

We also just treated animals with TCM or SFM without subsequently establishing primary tumors in them to determine only the “TCM effects” (or “SFM effects”) on pre-metastatic organs while avoiding the effects of the primary tumor and metastasized tumor cells in the organs. Treatment with TCM induced lymphangiogenesis in the lungs and the LN (Fig. 5) facilitating metastasis in these organs. The new lymphatic vessels in these organs might be connected to the rest of the lymphatic system and to the peritumoral lymphatics. The result might be an increased number of tumor cells that travel from the primary tumor to these organs and more metastasis. It is generally thought that the LN are mostly metastasized through the lymphatics as regional or sentinel LN are directly connected to the tumors through the lymphatic vessels [3]. However, TCM-induced lymphangiogenesis in the lungs that we report here is unusual as it is known that lungs are metastasized via the hematogenous route [10, 18]. Further studies are needed to investigate the role of increased lymphatics within the LN and lungs to accelerate metastasis.

According to the “seed and soil hypothesis”, metastatic cancer cells function as “seeds” and a particular organ microenvironment or niche serves as the “soil” [19]. The “soil” needs to

be conditioned to function as a metastatic niche ahead of actual metastasis [11]. We observed that TCM treatment induced neo-angiogenesis in LN and the enhanced angiogenesis is partly associated with phosphorylation of VEGFR-2 and EGFR (Figs. 6A and 6B). In recent reports tumor exosomes carrying tumor-derived cargo, including tumor-secreted factors (growth factors and cytokines), have been shown to be released by tumors to condition sentinel LN to be more angiogenic for tumor metastasis [20, 21]. These results suggest that TCM in our model could function like tumor-secreted exosomes as a cocktail of several tumor-derived factors to condition the LN. There needs to be further investigation into the key factors present in the TCM which are required for conditioning of the LN.

We also observed that TCM pre-treatment facilitated tumor cell spreading in the abdominal sites (Fig. 7C). The intra-abdominal metastasis was determined by comparing of the luminescent image and the light image without luminescent signals. If the animal has luminescent signals beyond the boundary of the primary tumors that is found in the light image, we counted that the animal has the intra-abdominal metastases. Primary tumors with a statistically identical size within two groups suggest that the different intra-abdominal metastasis rate was independent to the progression of primary tumors. The results above and the TCM-induced cancer cell motility data (Figs. 7A and 7B) can suggest that TCM pre-treatment might create a gradient of factors that enhance the chemotaxis of tumor cells in vivo, inducing them to disperse from the primary site. The increase in the intra-abdominal metastases generally facilitated metastasis to other organs such as liver, spleen, stomach, jejunal and duodenal segment of the intestine as shown in Figure 7C and is described in [22, 23].

We believe that pre-treatment with TCM to enhance metastasis has physiological relevance as a number of studies have employed conditioned media from solid tumor cells to understand mechanisms of tumor progression [24–29]. Primary tumors are probably always secreting factors, which would be equivalent to the TCM used here, into circulation. As tumors get larger, the concentrations of factors in this physiological TCM will increase. Also, even when the tumors are small and the concentrations of factors in the physiological TCM are low, the pre-metastatic sites are continuously being induced and prepared for the arrival of metastasized tumor cells. The continuous and long-term exposure to the factors may make up for the low concentrations of the factors physiologically. The question of why only specific sites in particular organs finally get colonized by the metastasized tumor cells when the whole body is exposed to the same tumor secreted factors remains unanswered. Moreover, adding a breast tumor mastectomy step to our current models needs to be explored as it can provide more clinically relevant perspectives when evaluating the efficacy of ant-metastatic or anti-angiogenic drugs after surgery as suggested in [30].

Collectively, our findings demonstrate that TCM pre-treatment enhances breast tumor metastasis in the LN and the lungs, showing enhanced lymphangiogenesis and angiogenesis in these organs. This model would allow the evaluation of anti-metastatic agents in a shorter time and with higher consistency.

Acknowledgments

We thank Zaver Bhujwalla for providing us with MDA-MB-231 and SUM-149 breast cancer cell lines for this study. This work was supported by the National Institutes of Health grant R01 CA138264, and grants from the Safeway Foundation for Breast Cancer and Maryland Technology Development Corporation (TEDCO).

Abbreviations

TCM	tumor-conditioned media

SFM	serum-free media
EGM	endothelial growth media
LN	lymph node
Ax-LN	axillary lymph node
Br-LN	brachial lymph node
LYVE-1	lymphatic vessel endothelial hyaluronan receptor-1
FITC	fluorescein isothiocyanate
DAPI	4',6-diamidino-2-phenylindole
anti-CK7	cytokeratin 7 antibody
anti-PCNA	proliferating cell nuclear antigen antibody
LEC	lymphatic endothelial cells
MEC	microvascular endothelial cell
GAPDH	glyceraldehyde 3-phosphate dehydrogenase
HEPES	4-(2-Hydroxyethyl)-1-piperazineethanesulfonic acid
TNBC	triple-negative breast cancer

References

1. Maehara Y, Tomisaki S, Oda S, et al. Lymph node metastasis and relation to tumor growth potential and local immune response in advanced gastric cancer. Int J Cancer. 1997; 74(2):224–228. [PubMed: 9133460]
2. Mori A, Arii S, Furutani M, et al. Vascular endothelial growth factor-induced tumor angiogenesis and tumorigenicity in relation to metastasis in a HT1080 human fibrosarcoma cell model. Int J Cancer. 1999; 80(5):738–743. [PubMed: 10048976]
3. Ran S, Volk L, Hall K, et al. Lymphangiogenesis and lymphatic metastasis in breast cancer. Pathophysiology. 2010; 17(4):229–251. [PubMed: 20036110]
4. Petrella BL. Assessment of local proteolytic milieu as a factor in tumor invasiveness and metastasis formation: in vitro collagen degradation and invasion assays. Methods Mol Biol. 2009; 511:75–84. [PubMed: 19347293]
5. Carlini MJ, De Lorenzo MS, Puricelli L. Cross-talk between tumor cells and the microenvironment at the metastatic niche. Curr Pharm Biotechnol. 2011; 12(11):1900–1908. [PubMed: 21470134]
6. Tammela T, Alitalo K. Lymphangiogenesis: Molecular mechanisms and future promise. Cell. 2010; 140(4):460–476. [PubMed: 20178740]
7. Alitalo K, Carmeliet P. Molecular mechanisms of lymphangiogenesis in health and disease. Cancer Cell. 2002; 1(3):219–227. [PubMed: 12086857]
8. Lee E, Koskimaki JE, Pandey NB, et al. Inhibition of lymphangiogenesis and angiogenesis in breast tumor xenografts and lymph nodes by a peptide derived from transmembrane protein 45A. Neoplasia. 2013; 15(2):112–124. [PubMed: 23441126]
9. Hirakawa S, Kodama S, Kunstfeld R, et al. VEGF-A induces tumor and sentinel lymph node lymphangiogenesis and promotes lymphatic metastasis. J Exp Med. 2005; 201(7):1089–1099. [PubMed: 15809353]
10. Wong CC, Zhang H, Gilkes DM, et al. Inhibitors of hypoxia-inducible factor 1 block breast cancer metastatic niche formation and lung metastasis. J Mol Med (Berl). 2012; 90(7):803–115. [PubMed: 22231744]
11. Psaila B, Lyden D. The metastatic niche: adapting the foreign soil. Nat Rev Cancer. 2009; 9(4): 285–293. [PubMed: 19308068]

12. Yamamoto M, Kikuchi H, Ohta M, et al. TSU68 prevents liver metastasis of colon cancer xenografts by modulating the premetastatic niche. Cancer Res. 2008; 68(23):9754–9762. [PubMed: 19047154]
13. Kim IS, Baek SH. Mouse models for breast cancer metastasis. Biochem Biophys Res Commun. 2010; 394(3):443–447. [PubMed: 20230796]
14. Francia G, Cruz-Munoz W, Man S, et al. Mouse models of advanced spontaneous metastasis for experimental therapeutics. Nat Rev Cancer. 2011; 11(2):135–141. [PubMed: 21258397]
15. Jenkins DE, Hornig YS, Oei Y, et al. Bioluminescent human breast cancer cell lines that permit rapid and sensitive in vivo detection of mammary tumors and multiple metastases in immune deficient mice. Breast Cancer Res. 2005; 7(4):R444–R454. [PubMed: 15987449]
16. Padua D, Zhang XH, Wang Q, et al. TGFbeta primes breast tumors for lung metastasis seeding through angiopoietin-like 4. Cell. 2008; 133(1):66–77. [PubMed: 18394990]
17. Padera TP, Kadambi A, di Tomaso E, et al. Lymphatic metastasis in the absence of functional intratumor lymphatics. Science. 2002; 296(5574):1883–1886. [PubMed: 11976409]
18. Hayashida T, Takahashi F, Chiba N, et al. HOXB9, a gene overexpressed in breast cancer, promotes tumorigenicity and lung metastasis. Proc Natl Acad Sci U S A. 2010; 107(3):1100–1105. [PubMed: 20080567]
19. Paget S. The distribution of secondary growths in cancer of the breast. 1889. Cancer Metastasis Rev. 1989; 8(2):98–101. [PubMed: 2673568]
20. Hood JL, San RS, Wickline SA. Exosomes released by melanoma cells prepare sentinel lymph nodes for tumor metastasis. Cancer Res. 2011; 71(11):3792–3801. [PubMed: 21478294]
21. Alderton GK. Metastasis. Exosomes drive premetastatic niche formation. Nat Rev Cancer. 2012; 12(7):447. [PubMed: 22722393]
22. Shih YJ, Hsu KF, Yu JC, et al. Synchronous hepatocellular carcinoma and sigmoid colon metastasis presenting as liver and intra-abdominal abscesses. Acta Gastroenterol Belg. 2012; 75(2):278–279. [PubMed: 22870798]
23. Rouhanimanesh Y, Vanderstighelen Y, Vanderputte S, et al. Intra-abdominal metastases from primary carcinoma of the lung. Acta Chir Belg. 2001; 101(6):300–303. [PubMed: 11868507]
24. Wason D, Richkind KE. The use of giant cell tumor conditioned media in cytogenetic studies of hematologic malignancies. Cancer Genet Cytogenet. 1992; 61(2):126–130. [PubMed: 1638490]
25. Festuccia C, Bologna M, Gravina GL, et al. Osteoblast conditioned media contain TGF-beta1 and modulate the migration of prostate tumor cells and their interactions with extracellular matrix components. Int J Cancer. 1999; 81(3):395–403. [PubMed: 10209954]
26. Michielsen AJ, O'Sullivan JN, Ryan EJ. Tumor conditioned media from colorectal cancer patients inhibits dendritic cell maturation. Oncoimmunology. 2012; 1(5):751–753. [PubMed: 22934271]
27. Burgess LC, Hall JO. Conditioned media from solid tumor cell lines treated with retinoic acids both decreases and increases proliferation of capillary endothelial cells. Life Sci. 2001; 69(24): 2819–2831. [PubMed: 11720086]
28. Kaplan RN, Riba RD, Zacharoulis S, et al. VEGFR1-positive haematopoietic bone marrow progenitors initiate the pre-metastatic niche. Nature. 2005; 438(7069):820–827. [PubMed: 16341007]
29. Mayorca-Guiliani AE, Yano H, Nakashiro K, et al. Premetastatic vasculogenesis in oral squamous cell carcinoma xenograft-draining lymph nodes. Oral Oncol. 2012; 48(8):663–670. [PubMed: 22401871]
30. Guerin E, Man S, Xu P, et al. A model of postsurgical advanced metastatic breast cancer more accurately replicates the clinical efficacy of antiangiogenic drugs. Cancer Res. 2013; 73(9):2743–2748. [PubMed: 23610448]

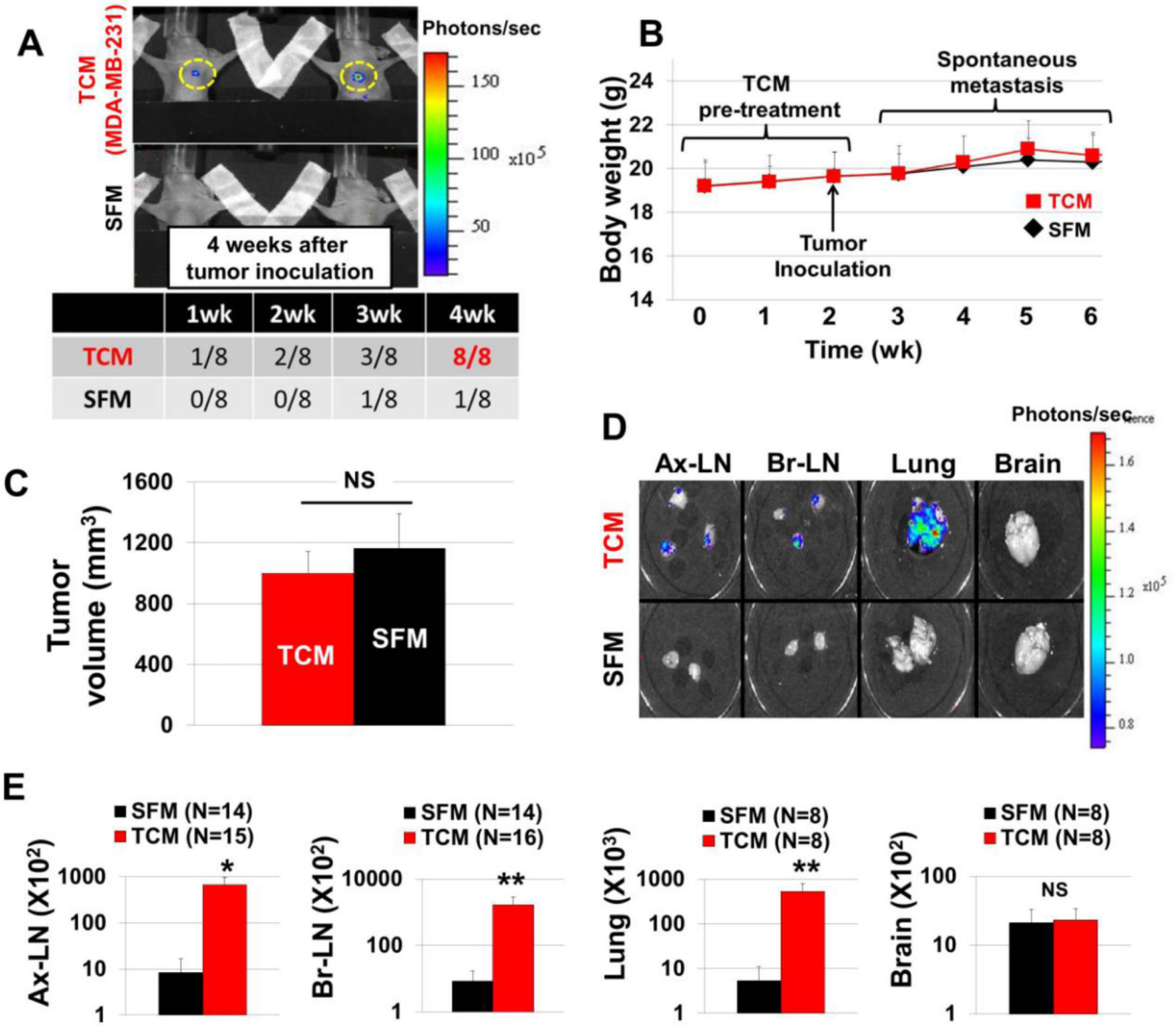

	1wk	2wk	3wk	4wk
TCM	1/8	2/8	3/8	8/8
SFM	0/8	0/8	1/8	1/8

Figure 1. Spontaneous MDA-MB-231 breast tumor metastasis model

(A) Anterior metastases in 4 weeks. The table shows the number of animals that exhibit anterior metastases at the end of every week for 4 weeks. **(B)** Animal body weight. No significant body weight changes were observed during the experiment suggesting that the tumor-conditioned media (TCM) does not cause severe toxicity of TCM in the animals. **(C)** Primary tumor sizes were determined after 4 weeks of tumor inoculation. There was no significant difference between TCM and serum-free media (SFM) treated groups. **(D)** Representative images of the organs (LN, lung, and brain) seen with the IVIS imager. **(E)** Metastatic flux in the LN, the lungs, and brains (**P < 0.01 and *P < 0.05).

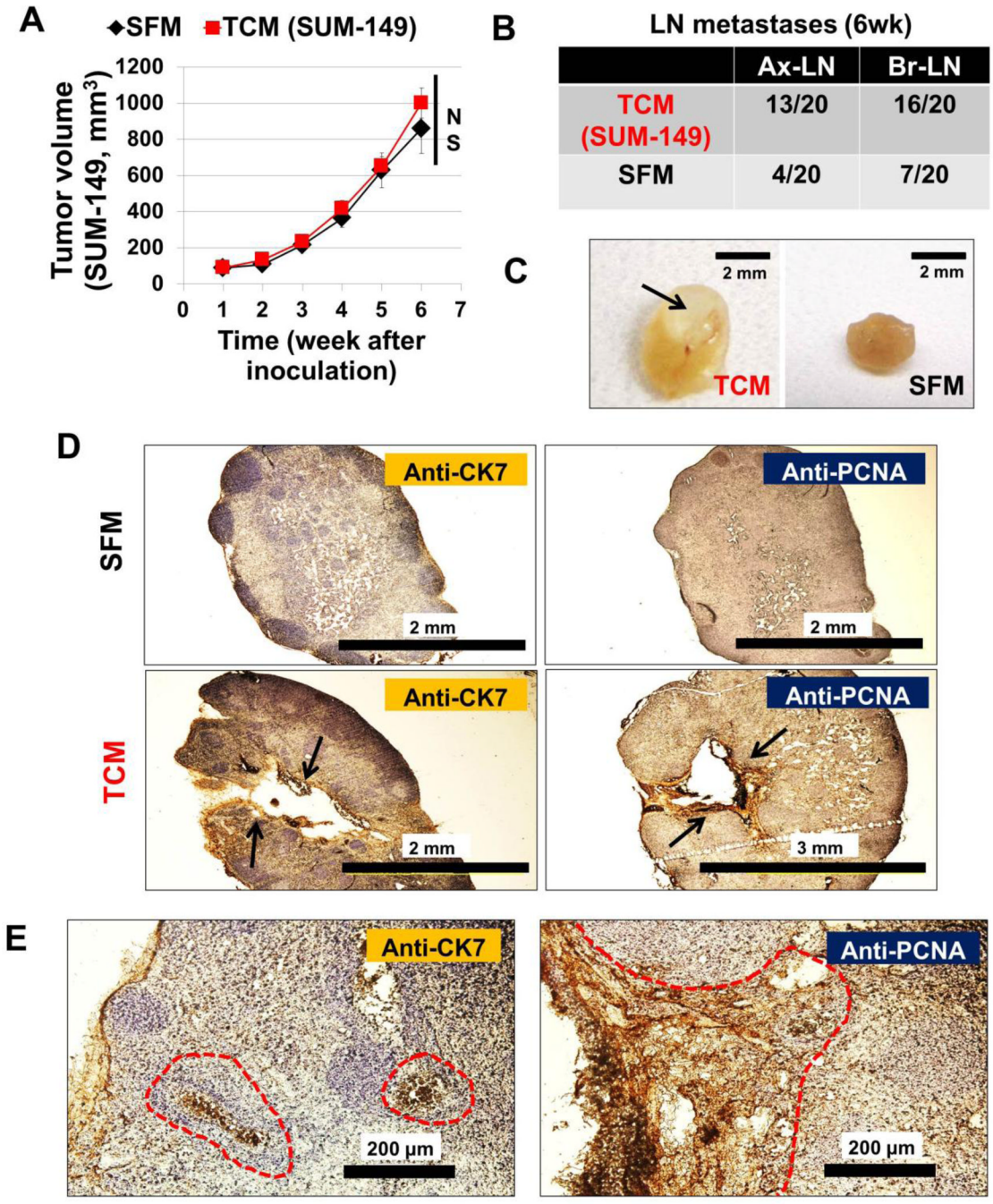

Figure 2. Spontaneous SUM-149 breast tumor LN metastasis

(A) SUM-149 primary tumor growth data. SUM-149 tumor growth was slower than MDA-MB-231 tumor growth in Figure 1, showing 1,000 mm^3 primary tumors after 6 weeks of SUM-149 tumor inoculation. There was no significant difference between TCM and SFM treated groups. **(B)** The number of the metastasized LN, which is determined by immunohistochemistry with anti-cytokeratin 7 (CK7) and anti-human PCNA. 2–3 times more LN were metastasized in TCM-treated group, compared to SFM-treated group. **(C)** Representative LN images. The black arrow represents lymphadenopathy (swollen LN with transparent fluid in the LN) in LN from TCM-treated animals. **(D)** Representative images of

DAB-mediated immunohistochemisty of LN sections with anti-CK7 and anti-PCNA. Hematoxylin was used for counterstaining. Black arrows represent metastatic tumor cells detected in TCM-treated LN. SFM-treated LN have fewer metastases and less lymphadenopathy, showing intact LN structure. However TCM-treated LN have empty spaces where the fluid used to be before sectioning of the swollen LN. Most tumor cells were detected around the area of lymphadenopathy. **(E)** Representative images of TCM-treated LN. CK7 and PCNA positive metastatic tumor cells are delineated by red-dotted curves.

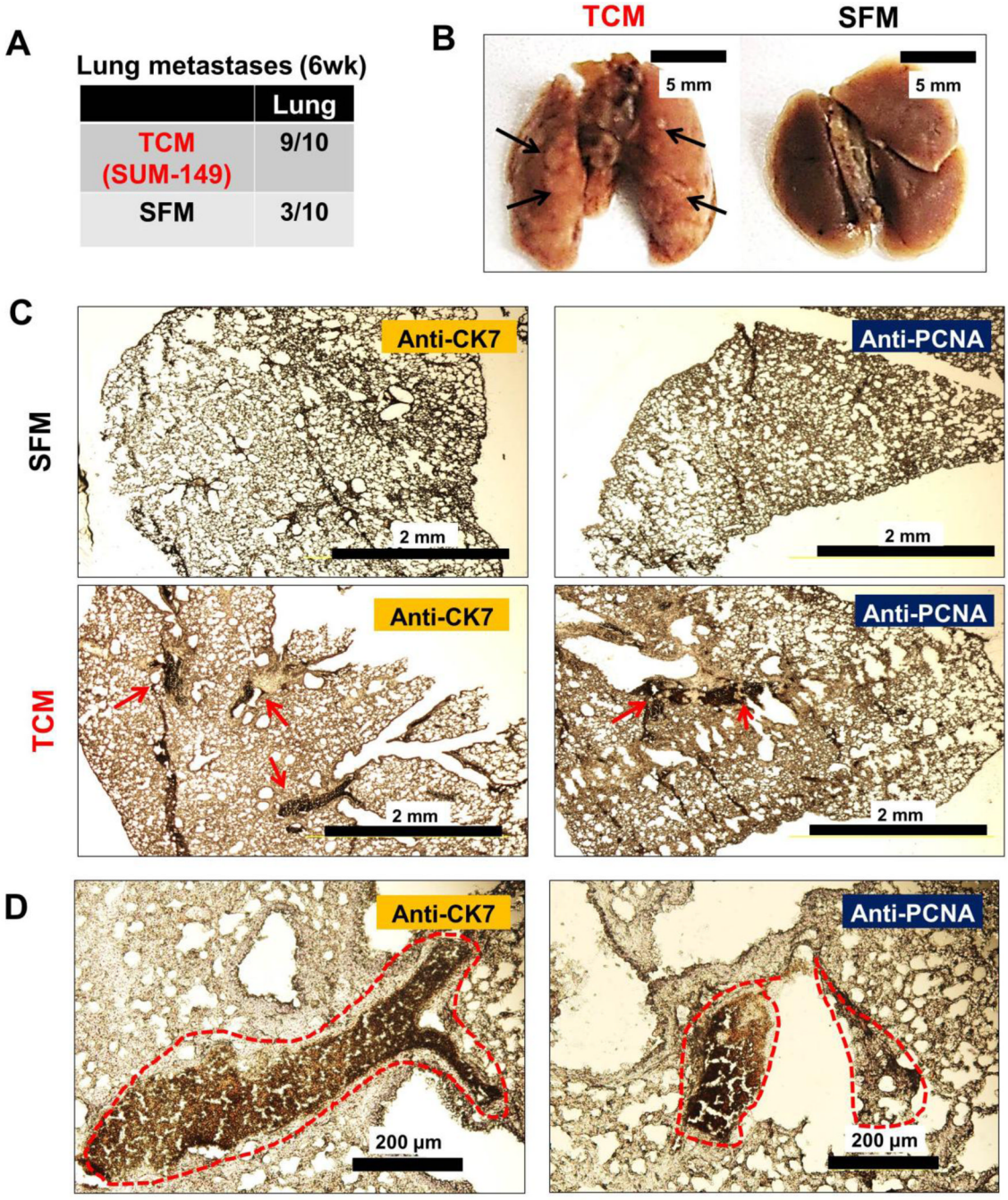

Figure 3. Spontaneous SUM-149 breast tumor lung metastasis

(A) The number of metastasized lungs as determined by immunohistochemistry with anti-CK7 and anti-human PCNA antibodies. 3 times as many lungs were metastasized in the TCM-treated group, compared to the SFM-treated group. **(B)** Representative lung images. Black arrows represent metastatic tumor nodules on the surface of the TCM-treated lungs. **(C)** Representative images of lung immunohistochemisty with anti-CK7 and anti-PCNA antibodies. Red arrows represent metastatic tumor cells detected in TCM-treated lungs. **(D)** Representative immunohistochemistry images of TCM-treated lungs. CK7 and PCNA positive metastatic tumor cells are delineated by red-dotted curves.

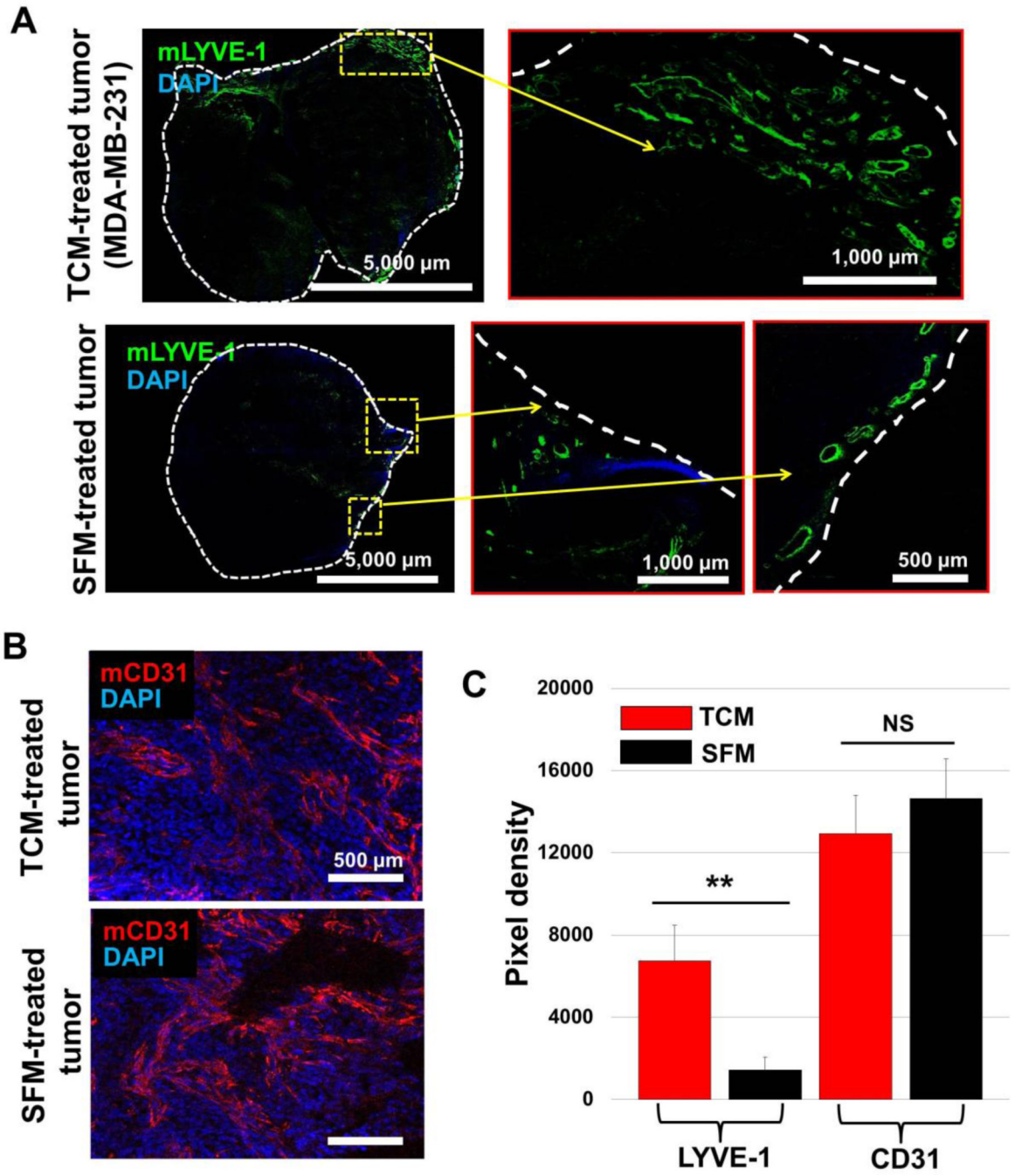

Figure 4. Changes in tumor microenvironment after TCM treatment

(A) The distribution of lymphatic vessels in tumors. TCM-treated animals showed enhanced peritumoral lymphangiogenesis compared to SFM-treated animals. Enlarged images show the presence of lumens in the lymphatic vessels. **(B)** Blood vessels in the tumor tissues. No significant change in angiogenesis was seen after TCM treatment. **(C)** Quantification of (A) and (B). ImageJ was used to quantify lymphatic vessels and blood vessels in the tumors. The lymphatic vessel density was increased 4.68 times upon TCM treatment. $^{**}P < 0.01$ versus SFM-treated control.

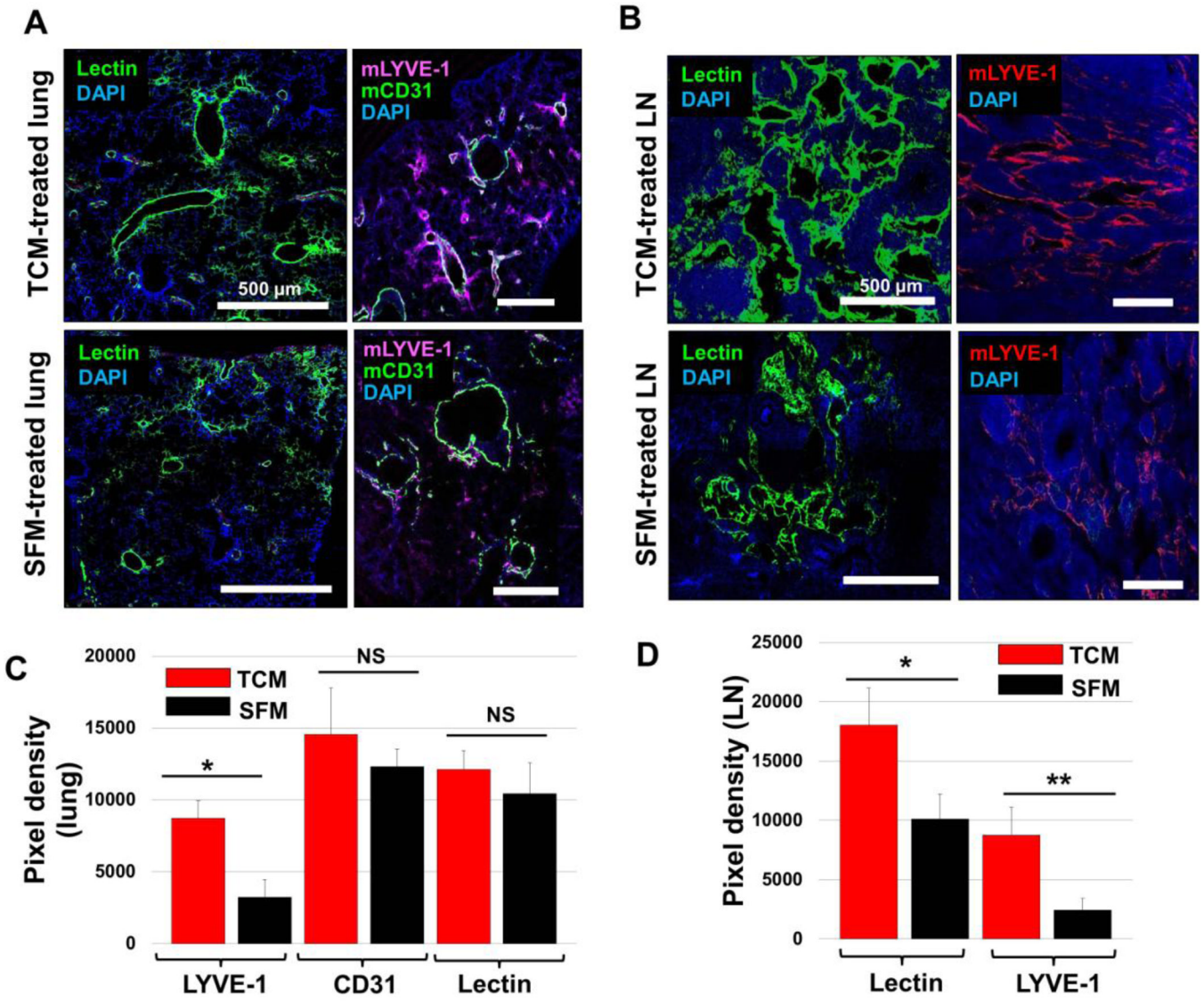

Figure 5. Changes in the lung and the LN microenvironment after TCM treatment

Lymphatic vessels (LYVE-1) and blood vessels (CD31 and lectin) were detected by immunofluorescence. **(A)** Representative images of the TCM or SFM-treated lungs. TCM-treated animals showed enhanced lymphangiogenesis in lungs compared to SFM-treated animals. However, angiogenesis was not influenced by TCM. **(B)** Lymphatic vessels and blood vessels within the LN. The TCM-treated animals showed enhanced lymphangiogenesis and angiogenesis in the LNs compared to the SFM-treated animals. **(C)** Quantification of (A). The lymphatic vessel density was increased by TCM (*$P < 0.05$). The blood vessel density, determined by anti-CD31 and anti-lectin staining, was not influenced by the TCM treatment. **(D)** Quantification of (B). The lymphatic vessel density was increased 3.20 times, and blood vessel density (by anti-lectin) was increased 1.74 times. (**$P < 0.01$ and *$P < 0.05$).

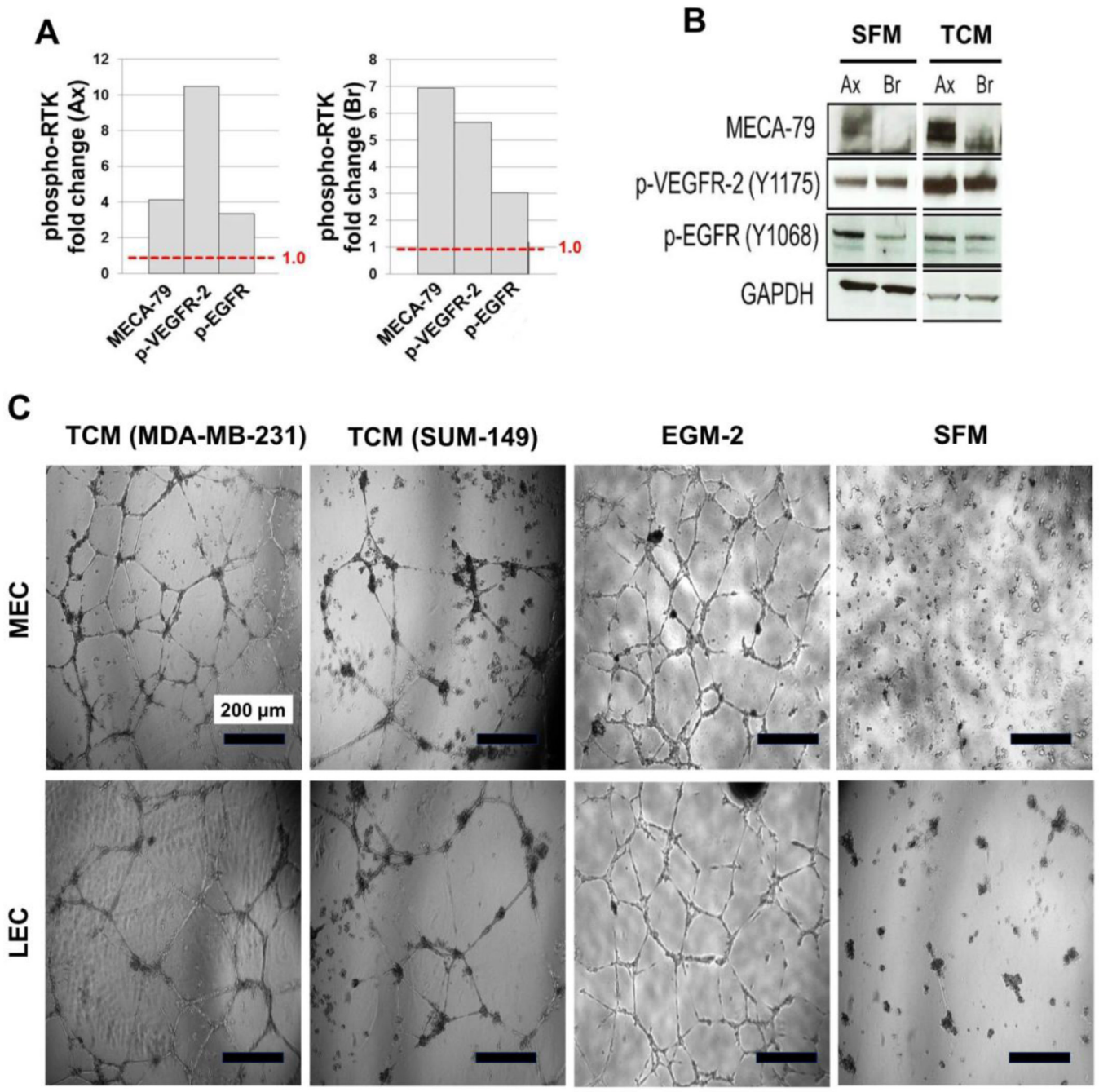

Figure 6. In vivo LN assays and in vitro tube formation

(A) Western blot assays were performed with tissue lysate prepared from TCM or SFM-treated axillary and brachial LN. Animals were dosed daily with 50 μl MDA-MB-231 tumor conditioned media (TCM) or serum-free media (SFM). After 14 days of administration, axillary and brachial lymph nodes (LN) were harvested, lysed, and probed with antibodies of interest including MECA-79, p-VEGFR-2 (Y1175), p-EGFR (Y1068), and GAPDH. Fold changes in these proteins after TCM treatment were obtained by measuring p-VEGFR-2, p-EGFR, and MECA-79 pixel density with the Image J. Red dotted lines (1.0-fold change) are shown as control (SFM-treated). **(B)** Western blot images. **(C)** Tumor-conditioned media (TCM) induced tube formation assays with microvascular and lymphatic endothelial cells

(MEC and LEC). TCM prepared from MDA-MB-231 and SUM-149 cells promote MEC/LEC tube formation. EGM-2 (normal endothelial media) and SFM were used as controls. Images were taken at 14 h after loading MEC and LEC.

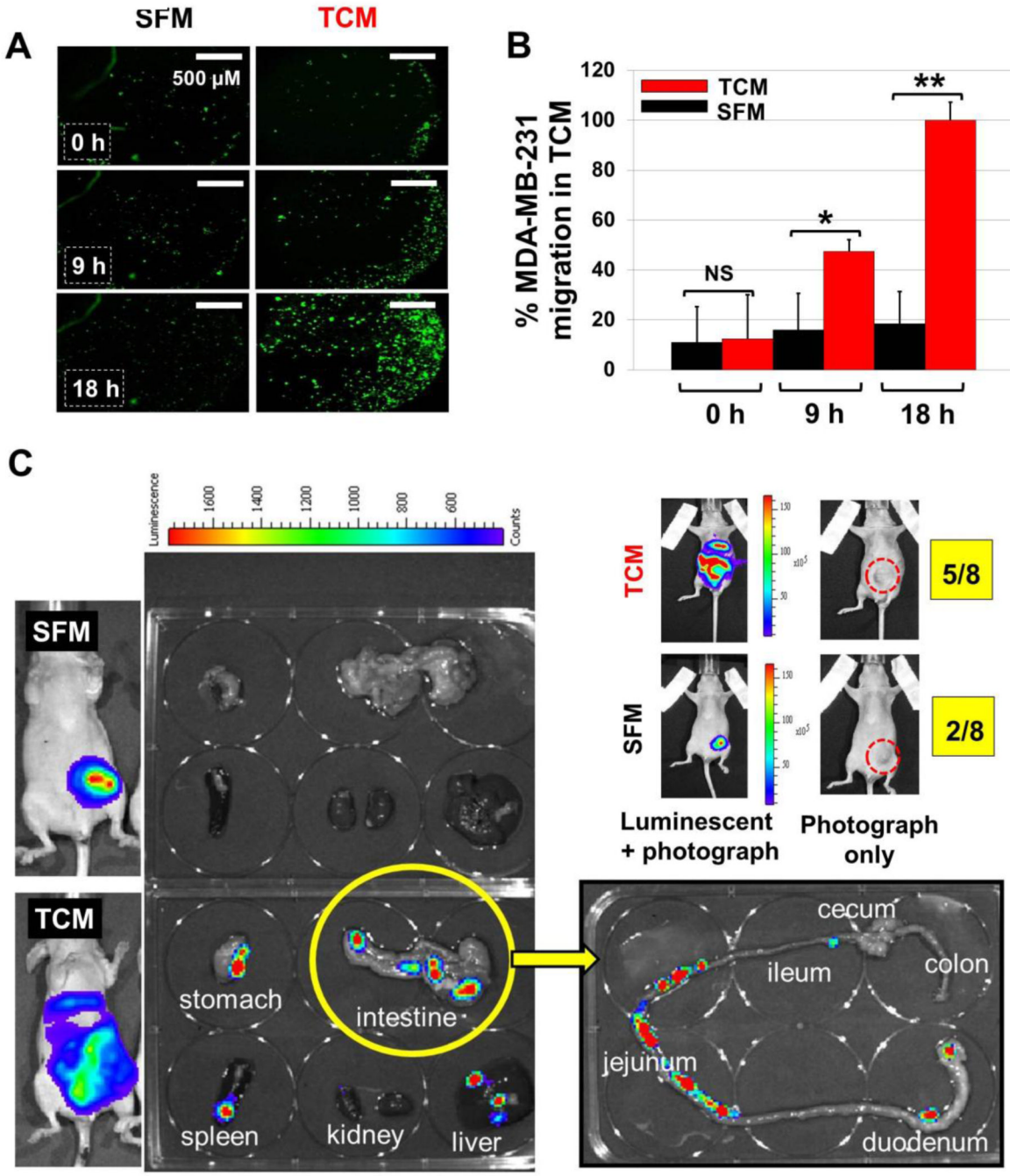

Figure 7. The effect of TCM on tumor cell motility and the intra-abdominal metastases

(A) Representative images of MDA-MB-231 tumor cell migration induced by MDA-MB-231 TCM or SFM at 0, 9, and 18 h. **(B)** Percent MDA-MB-231 migration in TCM. We set the extent of migration in TCM at 18 h as 100% migration (*$P < 0.05$ and **$P < 0.01$). **(C)** Representative images of the luminescent scan of the whole animals after 4 weeks of tumor inoculation. Luminescent images showed that TCM-treated animals had more intra-abdominal dissemination of tumor cells compared to SFM-treated animals. The yellow rectangle represents the intra-abdominal metastasis rate (a/b) after 4 weeks of tumor inoculation: ‘a’ is the number of animals with intra-abdominal metastases, and ‘b’ is the

total number of animals observed. Internal organs from the abdominal region were harvested and imaged by the IVIS imager, showing that the stomach, the spleen, the liver, jejunal and duodenal parts of the intestine were metastasized.